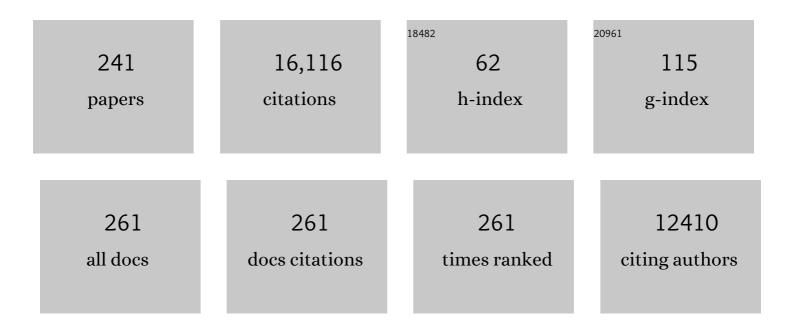
## **Richard Bowtell**

List of Publications by Year in descending order

Source: https://exaly.com/author-pdf/1752031/publications.pdf Version: 2024-02-01



#	Article	IF	CITATIONS
1	Magnetic Field Mapping and Correction for Moving OP-MEG. IEEE Transactions on Biomedical Engineering, 2022, 69, 528-536.	4.2	26
2	Magnetic field design in a cylindrical high-permeability shield: The combination of simple building blocks and a genetic algorithm. Journal of Applied Physics, 2022, 131, .	2.5	13
3	Triaxial detection of the neuromagnetic field using optically-pumped magnetometry: feasibility and application in children. NeuroImage, 2022, 252, 119027.	4.2	76
4	Using OPM-MEG in contrasting magnetic environments. NeuroImage, 2022, 253, 119084.	4.2	33
5	Phenotypic and genetic associations of quantitative magnetic susceptibility in UK Biobank brain imaging. Nature Neuroscience, 2022, 25, 818-831.	14.8	21
6	Bespoke magnetic field design for a magnetically shielded cold atom interferometer. Scientific Reports, 2022, 12, .	3.3	8
7	Magnetoencephalography with optically pumped magnetometers (OPM-MEG): the next generation of functional neuroimaging. Trends in Neurosciences, 2022, 45, 621-634.	8.6	91
8	A global survey of healthcare professionals undertaking MRI of patients with cochlear implants: a heterogeneity of practice and opinions. British Journal of Radiology, 2022, 95, .	2.2	0
9	Mouth magnetoencephalography: A unique perspective on the human hippocampus. NeuroImage, 2021, 225, 117443.	4.2	56
10	Probing the myelin water compartment with a saturationâ€recovery, multiâ€echo gradientâ€recalled echo sequence. Magnetic Resonance in Medicine, 2021, 86, 167-181.	3.0	2
11	Calibrationâ€free regional RF shims for MRS. Magnetic Resonance in Medicine, 2021, 86, 611-624.	3.0	4
12	Operculo-insular and anterior cingulate plasticity induced by transcranial magnetic stimulation in the human motor cortex: a dynamic casual modeling study. Journal of Neurophysiology, 2021, 125, 1180-1190.	1.8	9
13	Measuring functional connectivity with wearable MEG. NeuroImage, 2021, 230, 117815.	4.2	72
14	Planar Coil Optimization in a Magnetically Shielded Cylinder. Physical Review Applied, 2021, 15, .	3.8	13
15	Measuring the cortical tracking of speech with optically-pumped magnetometers. NeuroImage, 2021, 233, 117969.	4.2	22
16	Beta-frequency electrophysiological bursts: BOLD correlates and relationships with psychotic illness. BJPsych Open, 2021, 7, S37-S38.	0.7	0
17	Parametric Assessment of the Effect of Cochlear Implant Positioning on Brain MRI Artefacts at 3 T. Otology and Neurotology, 2021, 42, e1449-e1456.	1.3	3
18	Theoretical advantages of a triaxial optically pumped magnetometer magnetoencephalography system. Neurolmage, 2021, 236, 118025.	4.2	73

#	Article	IF	CITATIONS
19	Practical real-time MEG-based neural interfacing with optically pumped magnetometers. BMC Biology, 2021, 19, 158.	3.8	14
20	Precision magnetic field modelling and control for wearable magnetoencephalography. NeuroImage, 2021, 241, 118401.	4.2	54
21	Optimised hybrid shielding and magnetic field control for emerging quantum technologies. , 2021, , .		2
22	Design and testing of microbubbleâ€based MRI contrast agents for gastric pressure measurement. Magnetic Resonance in Medicine, 2020, 83, 1096-1108.	3.0	1
23	Multi-site harmonization of 7 tesla MRI neuroimaging protocols. NeuroImage, 2020, 206, 116335.	4.2	36
24	Optimal Inverse Design of Magnetic Field Profiles in a Magnetically Shielded Cylinder. Physical Review Applied, 2020, 14, .	3.8	24
25	Pragmatic spatial sampling for wearable MEG arrays. Scientific Reports, 2020, 10, 21609.	3.3	23
26	Multi-centre, multi-vendor reproducibility of 7T QSM and R2* in the human brain: Results from the UK7T study. NeuroImage, 2020, 223, 117358.	4.2	20
27	Regional Brain Correlates of Beta Bursts in Health and Psychosis: A Concurrent Electroencephalography and Functional Magnetic Resonance Imaging Study. Biological Psychiatry: Cognitive Neuroscience and Neuroimaging, 2020, 6, 1145-1156.	1.5	6
28	The haemodynamics of the human placenta in utero. PLoS Biology, 2020, 18, e3000676.	5.6	37
29	Multi-channel whole-head OPM-MEG: Helmet design and a comparison with a conventional system. NeuroImage, 2020, 219, 116995.	4.2	164
30	Strong diffusion gradients allow the separation of intra- and extra-axonal gradient-echo signals in the human brain. NeuroImage, 2020, 217, 116793.	4.2	21
31	Modulating Brain Networks With Transcranial Magnetic Stimulation Over the Primary Motor Cortex: A Concurrent TMS/fMRI Study. Frontiers in Human Neuroscience, 2020, 14, 31.	2.0	36
32	Optically pumped magnetoencephalography in epilepsy. Annals of Clinical and Translational Neurology, 2020, 7, 397-401.	3.7	43
33	The haemodynamics of the human placenta in utero. , 2020, 18, e3000676.		0
34	The haemodynamics of the human placenta in utero. , 2020, 18, e3000676.		0
35	The haemodynamics of the human placenta in utero. , 2020, 18, e3000676.		0
36	The haemodynamics of the human placenta in utero. , 2020, 18, e3000676.		0

The haemodynamics of the human placenta in utero. , 2020, 18, e3000676. 36

#	Article	IF	CITATIONS
37	The haemodynamics of the human placenta in utero. , 2020, 18, e3000676.		Ο
38	The haemodynamics of the human placenta in utero. , 2020, 18, e3000676.		0
39	Wearable neuroimaging: Combining and contrasting magnetoencephalography and electroencephalography. NeuroImage, 2019, 201, 116099.	4.2	82
40	European Ultrahighâ€Field Imaging Network for Neurodegenerative Diseases (EUFIND). Alzheimer's and Dementia: Diagnosis, Assessment and Disease Monitoring, 2019, 11, 538-549.	2.4	17
41	Dataâ€driven model optimization for optically pumped magnetometer sensor arrays. Human Brain Mapping, 2019, 40, 4357-4369.	3.6	16
42	Simultaneous EEG-fMRI: Evaluating the Effect of the EEG Cap-Cabling Configuration on the Gradient Artifact. Frontiers in Neuroscience, 2019, 13, 690.	2.8	7
43	Using optically pumped magnetometers to measure magnetoencephalographic signals in the human cerebellum. Journal of Physiology, 2019, 597, 4309-4324.	2.9	31
44	Phase enhanced PSIR T1 weighted imaging improves contrast resolution of the nucleus basalis of Meynert at 7â€T: a preliminary study. Magnetic Resonance Imaging, 2019, 61, 296-299.	1.8	5
45	Balanced, bi-planar magnetic field and field gradient coils for field compensation in wearable magnetoencephalography. Scientific Reports, 2019, 9, 14196.	3.3	72
46	A tool for functional brain imaging with lifespan compliance. Nature Communications, 2019, 10, 4785.	12.8	96
47	Imaging the human hippocampus with optically-pumped magnetoencephalography. NeuroImage, 2019, 203, 116192.	4.2	52
48	Optically pumped magnetometers: From quantum origins to multi-channel magnetoencephalography. NeuroImage, 2019, 199, 598-608.	4.2	186
49	Towards OPM-MEG in a virtual reality environment. NeuroImage, 2019, 199, 408-417.	4.2	87
50	Updating Dynamic Noise Models With Moving Magnetoencephalographic (MEG) Systems. IEEE Access, 2019, 7, 10093-10102.	4.2	5
51	Frequency difference mapping applied to the corpus callosum at 7T. Magnetic Resonance in Medicine, 2019, 81, 3017-3031.	3.0	20
52	Reference Layer Artefact Subtraction (RLAS): Electromagnetic Simulations. IEEE Access, 2019, 7, 17882-17895.	4.2	5
53	ls Human Auditory Cortex Organization Compatible With the Monkey Model? Contrary Evidence From Ultra-High-Field Functional and Structural MRI. Cerebral Cortex, 2019, 29, 410-428.	2.9	16
54	Exploring the relative efficacy of motion artefact correction techniques for EEG data acquired during simultaneous fMRI. Human Brain Mapping, 2019, 40, 578-596.	3.6	12

#	Article	IF	CITATIONS
55	Exploring the origins of EEG motion artefacts during simultaneous fMRI acquisition: Implications for motion artefact correction. NeuroImage, 2018, 173, 188-198.	4.2	11
56	Moving magnetoencephalography towards real-world applications with a wearable system. Nature, 2018, 555, 657-661.	27.8	795
57	Microstructural imaging of the human brain with a â€̃super-scanner': 10 key advantages of ultra-strong gradients for diffusion MRI. NeuroImage, 2018, 182, 8-38.	4.2	138
58	Cognitive neuroscience using wearable magnetometer arrays: Non-invasive assessment of language function. Neurolmage, 2018, 181, 513-520.	4.2	56
59	Quantifying MRI frequency shifts due to structures with anisotropic magnetic susceptibility using pyrolytic graphite sheet. Scientific Reports, 2018, 8, 6259.	3.3	6
60	A bi-planar coil system for nulling background magnetic fields in scalp mounted magnetoencephalography. NeuroImage, 2018, 181, 760-774.	4.2	143
61	A new generation of magnetoencephalography: Room temperature measurements using optically-pumped magnetometers. NeuroImage, 2017, 149, 404-414.	4.2	329
62	Editorial for special issue on MRI phase contrast and quantitative susceptibility mapping. NMR in Biomedicine, 2017, 30, e3707.	2.8	2
63	Histological Basis of Laminar MRI Patterns in High Resolution Images of Fixed Human Auditory Cortex. Frontiers in Neuroscience, 2016, 10, 455.	2.8	21
64	Vertex Stimulation as a Control Site for Transcranial Magnetic Stimulation: A Concurrent TMS/fMRI Study. Brain Stimulation, 2016, 9, 58-64.	1.6	100
65	A comparison of phase imaging and quantitative susceptibility mapping in the imaging of multiple sclerosis lesions at ultrahigh field. Magnetic Resonance Materials in Physics, Biology, and Medicine, 2016, 29, 543-557.	2.0	38
66	Global signal modulation of single-trial fMRI response variability: Effect on positive vs negative BOLD response relationship. NeuroImage, 2016, 133, 62-74.	4.2	22
67	MRI illuminated by γ-rays. Nature, 2016, 537, 621-622.	27.8	1
68	On the Potential of a New Generation of Magnetometers for MEG: A Beamformer Simulation Study. PLoS ONE, 2016, 11, e0157655.	2.5	138
69	Mapping quantal touch using 7 Tesla functional magnetic resonance imaging and single-unit intraneural microstimulation. ELife, 2016, 5, .	6.0	33
70	Effects of white matter microstructure on phase and susceptibility maps. Magnetic Resonance in Medicine, 2015, 73, spcone-spcone.	3.0	0
71	Effects of white matter microstructure on phase and susceptibility maps. Magnetic Resonance in Medicine, 2015, 73, 1258-1269.	3.0	116
72	Increase in the iron content of the substantia nigra and red nucleus in multiple sclerosis and clinically isolated syndrome: A 7 Tesla MRI study. Journal of Magnetic Resonance Imaging, 2015, 41, 1065-1070.	3.4	37

#	Article	IF	CITATIONS
73	Simultaneous EEG–fMRI: evaluating the effect of the cabling configuration on the gradient artefact. Physics in Medicine and Biology, 2015, 60, N241-N250.	3.0	15
74	Assessing the Spatial Precision of SE and GE-BOLD Contrast at 7 Tesla. Brain Topography, 2015, 28, 62-65.	1.8	14
75	Investigating the effect of modifying the EEG cap lead configuration on the gradient artifact in simultaneous EEG-fMRI. Frontiers in Neuroscience, 2014, 8, 226.	2.8	6
76	Global intravascular and local hyperoxia contrast phase-based blood oxygenation measurements. NeuroImage, 2014, 101, 458-465.	4.2	9
77	Eventâ€related fMRI at 7T reveals overlapping cortical representations for adjacent fingertips in S1 of individual subjects. Human Brain Mapping, 2014, 35, 2027-2043.	3.6	77
78	Evidence that the negative BOLD response is neuronal in origin: A simultaneous EEG–BOLD–CBF study in humans. NeuroImage, 2014, 94, 263-274.	4.2	137
79	Reference layer artefact subtraction (RLAS): A novel method of minimizing EEG artefacts during simultaneous fMRI. NeuroImage, 2014, 84, 307-319.	4.2	88
80	Neuroimaging paradigms for tonotopic mapping (I): The influence of sound stimulus type. NeuroImage, 2014, 100, 650-662.	4.2	18
81	Functional quantitative susceptibility mapping (fQSM). NeuroImage, 2014, 100, 112-124.	4.2	76
82	Regional structural differences across functionally parcellated Brodmann areas of human primary somatosensory cortex. Neurolmage, 2014, 93, 221-230.	4.2	55
83	Investigating intrinsic connectivity networks using simultaneous BOLD and CBF measurements. NeuroImage, 2014, 99, 111-121.	4.2	14
84	Theta power during encoding predicts subsequentâ€memory performance and default mode network deactivation. Human Brain Mapping, 2013, 34, 2929-2943.	3.6	79
85	A priori â€driven multivariate statistical approach to reduce dimensionality of MEG signals. Electronics Letters, 2013, 49, 1123-1124.	1.0	1
86	Identifying the sources of the pulse artefact in EEG recordings made inside an MR scanner. NeuroImage, 2013, 71, 75-83.	4.2	66
87	Gradient echo based fiber orientation mapping using R2* and frequency difference measurements. NeuroImage, 2013, 83, 1011-1023.	4.2	71
88	Single-subject fMRI mapping at 7 T of the representation of fingertips in S1: a comparison of event-related and phase-encoding designs. Journal of Neurophysiology, 2013, 109, 2293-2305.	1.8	75
89	Increased iron accumulation occurs in the earliest stages of demyelinating disease: an ultra-high field susceptibility mapping study in Clinically Isolated Syndrome. Multiple Sclerosis Journal, 2013, 19, 896-903.	3.0	83
90	Visualization of nigrosome 1 and its loss in PD. Neurology, 2013, 81, 534-540.	1.1	208

#	Article	IF	CITATIONS
91	Poststimulus undershoots in cerebral blood flow and BOLD fMRI responses are modulated by poststimulus neuronal activity. Proceedings of the National Academy of Sciences of the United States of America, 2013, 110, 13636-13641.	7.1	83
92	Best Current Practice for Obtaining High Quality EEG Data During Simultaneous fMRI. Journal of Visualized Experiments, 2013, , .	0.3	32
93	Calculation of the electric field resulting from human body rotation in a magnetic field. Physics in Medicine and Biology, 2012, 57, 4739-4753.	3.0	19
94	Fiber orientation-dependent white matter contrast in gradient echo MRI. Proceedings of the National Academy of Sciences of the United States of America, 2012, 109, 18559-18564.	7.1	294
95	Within-Digit Functional Parcellation of Brodmann Areas of the Human Primary Somatosensory Cortex Using Functional Magnetic Resonance Imaging at 7 Tesla. Journal of Neuroscience, 2012, 32, 15815-15822.	3.6	118
96	Motion-related artefacts in EEG predict neuronally plausible patterns of activation in fMRI data. NeuroImage, 2012, 59, 261-270.	4.2	56
97	Direct visualization of the subthalamic nucleus and its iron distribution using highâ€resolution susceptibility mapping. Human Brain Mapping, 2012, 33, 2831-2842.	3.6	91
98	Spatial location and strength of BOLD activation in highâ€spatialâ€resolution fMRI of the motor cortex: a comparison of spin echo and gradient echo fMRI at 7 T. NMR in Biomedicine, 2012, 25, 717-725.	2.8	35
99	Ultrahigh field systems and applications at 7 T and beyond: Progress, pitfalls, and potential. Magnetic Resonance in Medicine, 2012, 67, 317-321.	3.0	29
100	High resolution magnetic susceptibility mapping of the substantia nigra in Parkinson's disease. Journal of Magnetic Resonance Imaging, 2012, 35, 48-55.	3.4	189
101	Correspondence of human visual areas identified using functional and anatomical MRI in vivo at 7 T. Journal of Magnetic Resonance Imaging, 2012, 35, 287-299.	3.4	51
102	Combining EEG and fMRI. Methods in Molecular Biology, 2011, 711, 303-326.	0.9	38
103	Reducing the gradient artefact in simultaneous EEC-fMRI by adjusting the subject's axial position. NeuroImage, 2011, 54, 1942-1950.	4.2	64
104	Structural properties of the corticospinal tract in the human brain: a magnetic resonance imaging study at 7 Tesla. Brain Structure and Function, 2011, 216, 255-262.	2.3	14
105	PEG coating reduces NMR relaxivity of <i>Mn</i> <sub>0.5</sub> <i>Zn</i> <sub>0.5</sub> <i>Gd</i> <sub>0.02</sub> <i>Fe</i> <sub>1.98</sub> <i nanoparticles. Journal of Magnetic Resonance Imaging, 2011, 34, 1192-1198.</i 	>O <b>ଃ/i</b> ≯≺su	b> <b>4</b> 8/sub>hy
106	Reducing peripheral nerve stimulation due to gradient switching using an additional uniform field coil. Magnetic Resonance in Medicine, 2011, 66, 1498-1509.	3.0	9
107	Physical modeling of pulse artefact sources in simultaneous EEG/fMRI. Human Brain Mapping, 2010, 31, 604-620.	3.6	55
108	Mapping Human Somatosensory Cortex in Individual Subjects With 7T Functional MRI. Journal of Neurophysiology, 2010, 103, 2544-2556.	1.8	197

#	Article	IF	CITATIONS
109	Brain Activations in Response to Vibrotactile Tooth Stimulation: a Psychophysical and fMRI Study. Journal of Neurophysiology, 2010, 104, 2257-2265.	1.8	59
110	Quantification of blood velocity and flow rates in the uterine vessels using echo planar imaging at 0.5 Tesla. Journal of Magnetic Resonance Imaging, 2010, 31, 921-927.	3.4	11
111	Susceptibility mapping in the human brain using thresholdâ€based <i>k</i> â€space division. Magnetic Resonance in Medicine, 2010, 63, 1292-1304.	3.0	229
112	Whole-brain susceptibility mapping at high field: A comparison of multiple- and single-orientation methods. NeuroImage, 2010, 53, 515-525.	4.2	172
113	A comparison of fMRI adaptation and multivariate pattern classification analysis in visual cortex. NeuroImage, 2010, 49, 1632-1640.	4.2	61
114	Investigating the effect of blood susceptibility on phase contrast in the human brain. NeuroImage, 2010, 50, 491-498.	4.2	28
115	2.4 Influence of EEG Equipment on MR Image Quality. , 2010, , 107-118.		1
116	Safety Implications of High-Field MRI: Actuation of Endogenous Magnetic Iron Oxides in the Human Body. PLoS ONE, 2009, 4, e5431.	2.5	11
117	A functional-magnetic-resonance-imaging investigation of cortical activation from moving vibrotactile stimuli on the fingertip. Journal of the Acoustical Society of America, 2009, 125, 1033-1039.	1.1	50
118	Split gradient coils for simultaneous PETâ€MRI. Magnetic Resonance in Medicine, 2009, 62, 1106-1111.	3.0	32
119	MRI rides the wave. Nature, 2009, 457, 971-972.	27.8	7
120	Phase vs. magnitude information in functional magnetic resonance imaging time series: toward understanding the noise. Magnetic Resonance Imaging, 2009, 27, 1046-1057.	1.8	40
121	Forward electric field calculation using BEM for time-varying magnetic field gradients and motion in strong static fields. Engineering Analysis With Boundary Elements, 2009, 33, 1074-1088.	3.7	26
122	fMRI analysis of active, passive and electrically stimulated ankle dorsiflexion. NeuroImage, 2009, 44, 469-479.	4.2	106
123	Source localisation in concurrent EEG/fMRI: Applications at 7T. NeuroImage, 2009, 45, 440-452.	4.2	32
124	Understanding gradient artefacts in simultaneous EEG/fMRI. NeuroImage, 2009, 46, 459-471.	4.2	56
125	fMRI at 1.5, 3 and 7 T: Characterising BOLD signal changes. NeuroImage, 2009, 47, 1425-1434.	4.2	240
126	Using magnetic field simulation to study susceptibility-related phase contrast in gradient echo MRI. Neurolmage, 2009, 48, 126-137.	4.2	108

#	Article	IF	CITATIONS
127	Exploring the feasibility of simultaneous electroencephalography/functional magnetic resonance imaging at 7 T. Magnetic Resonance Imaging, 2008, 26, 968-977.	1.8	53
128	High resolution SE-fMRI in humans at 3 and 7 T using a motor task. Magnetic Resonance Materials in Physics, Biology, and Medicine, 2008, 21, 113-120.	2.0	20
129	Volume parcellation for improved dynamic shimming. Magnetic Resonance Materials in Physics, Biology, and Medicine, 2008, 21, 31-40.	2.0	34
130	Water proton T 1 measurements in brain tissue at 7, 3, and 1.5T using IR-EPI, IR-TSE, and MPRAGE: results and optimization. Magnetic Resonance Materials in Physics, Biology, and Medicine, 2008, 21, 121-130.	2.0	222
131	Improved artifact correction for combined electroencephalography/functional MRI by means of synchronization and use of vectorcardiogram recordings. Journal of Magnetic Resonance Imaging, 2008, 27, 607-616.	3.4	65
132	Modeling and optimization of lookâ€locker spin labeling for measuring perfusion and transit time changes in activation studies taking into account arterial blood volume. Magnetic Resonance in Medicine, 2008, 59, 316-325.	3.0	56
133	Numerical solution for an inverse MRI problem using a regularised boundary element method. Engineering Analysis With Boundary Elements, 2008, 32, 658-675.	3.7	6
134	Colourful future for MRI. Nature, 2008, 453, 993-994.	27.8	11
135	Measurement of electric fields induced in a human subject due to natural movements in static magnetic fields or exposure to alternating magnetic field gradients. Physics in Medicine and Biology, 2008, 53, 361-373.	3.0	36
136	Properties of the ballistocardiogram artefact as revealed by EEG recordings at 1.5, 3 and 7 T static magnetic field strength. International Journal of Psychophysiology, 2008, 67, 189-199.	1.0	182
137	Effects of simultaneous EEG recording on MRI data quality at 1.5, 3 and 7Âtesla. International Journal of Psychophysiology, 2008, 67, 178-188.	1.0	73
138	Simultaneous EEG source localisation and artifact rejection during concurrent fMRI by means of spatial filtering. NeuroImage, 2008, 40, 1090-1104.	4.2	65
139	A novel MR-compatible device for providing forces to the human finger during functional neuroimaging studies. NeuroImage, 2008, 40, 1731-1737.	4.2	3
140	Theoretical optimization of multi-echo fMRI data acquisition. Physics in Medicine and Biology, 2007, 52, 1801-1813.	3.0	58
141	Electric fields induced in the human body by time-varying magnetic field gradients in MRI: numerical calculations and correlation analysis. Physics in Medicine and Biology, 2007, 52, 2337-2353.	3.0	49
142	Measurement of electric fields due to time-varying magnetic field gradients using dipole probes. Physics in Medicine and Biology, 2007, 52, 5119-5130.	3.0	26
143	Magnetic-field-induced vertigo: A theoretical and experimental investigation. Bioelectromagnetics, 2007, 28, 349-361.	1.6	165
144	Novel gradient coils designed using a boundary element method. Concepts in Magnetic Resonance Part B, 2007, 31B, 162-175.	0.7	144

#	Article	IF	CITATIONS
145	Thresholds for perceiving metallic taste at high magnetic field. Journal of Magnetic Resonance Imaging, 2007, 26, 1357-1361.	3.4	50
146	T2* measurements in human brain at 1.5, 3 and 7 T. Magnetic Resonance Imaging, 2007, 25, 748-753.	1.8	198
147	Sensitivity to local dipole fields in the CRAZED experiment: An approach to bright spot MRI. Journal of Magnetic Resonance, 2006, 182, 315-324.	2.1	33
148	Echo-shifted multislice EPI for high-speed fMRI. Magnetic Resonance Imaging, 2006, 24, 433-442.	1.8	12
149	Improved echo volumar imaging (EVI) for functional MRI. Magnetic Resonance in Medicine, 2006, 56, 1320-1327.	3.0	36
150	Pharmaceutical applications of magnetic resonance imaging (MRI). Advanced Drug Delivery Reviews, 2005, 57, 1191-1209.	13.7	186
151	Application of a Fourier-based method for rapid calculation of field inhomogeneity due to spatial variation of magnetic susceptibility. Concepts in Magnetic Resonance Part B, 2005, 25B, 65-78.	0.7	347
152	Hemispherical gradient coils for magnetic resonance imaging. Magnetic Resonance in Medicine, 2005, 54, 656-668.	3.0	20
153	Intermolecular multiple quantum coherences at high magnetic field: The nonlinear regime. Journal of Chemical Physics, 2005, 123, 164311.	3.0	12
154	Localised mapping of water movement and hydration inside a developing bioadhesive bond. Journal of Controlled Release, 2004, 95, 435-446.	9.9	13
155	Correction of spatial distortion in EPI due to inhomogeneous static magnetic fields using the reversed gradient method. Journal of Magnetic Resonance Imaging, 2004, 19, 499-507.	3.4	159
156	Optimizing the sequence parameters for double-quantum CRAZED imaging. Magnetic Resonance in Medicine, 2004, 51, 148-157.	3.0	26
157	Initial attempts at directly detecting alpha wave activity in the brain using MRI. Magnetic Resonance Imaging, 2004, 22, 1413-1427.	1.8	45
158	Investigating the coating-dependent release mechanism of a pulsatile capsule using NMR microscopy. Journal of Controlled Release, 2003, 92, 341-347.	9.9	30
159	Multilayer transverse gradient coil design. Concepts in Magnetic Resonance, 2003, 16B, 38-46.	1.3	22
160	MR tagging of human lungs using hyperpolarized3He gas. Journal of Magnetic Resonance Imaging, 2003, 17, 142-146.	3.4	57
161	Abnormal cortical sensory activation in dystonia: An fMRI study. Movement Disorders, 2003, 18, 673-682.	3.9	128
162	MRI detection of weak magnetic fields due to an extended current dipole in a conducting sphere: A model for direct detection of neuronal currents in the brain. Magnetic Resonance in Medicine, 2003, 50, 40-49.	3.0	88

#	Article	IF	CITATIONS
163	Using the vector potential in evaluating the likelihood of peripheral nerve stimulation due to switched magnetic field gradients. Magnetic Resonance in Medicine, 2003, 50, 405-410.	3.0	13
164	Actively shielded multi-layer gradient coil designs with improved cooling properties. Journal of Magnetic Resonance, 2003, 165, 196-207.	2.1	18
165	Representations of Pleasant and Painful Touch in the Human Orbitofrontal and Cingulate Cortices. Cerebral Cortex, 2003, 13, 308-317.	2.9	432
166	NMR imaging and structure measurements using the long-range dipolar field in liquids. Physical Review E, 2002, 66, 041201.	2.1	19
167	Electric fields induced in a spherical volume conductor by temporally varying magnetic field gradients. Physics in Medicine and Biology, 2002, 47, 557-576.	3.0	24
168	Functional neuroimaging studies of human somatosensory cortex. Behavioural Brain Research, 2002, 135, 147-158.	2.2	116
169	Mapping the absolute value ofMO using dipolar field effects. Magnetic Resonance in Medicine, 2002, 47, 871-879.	3.0	37
170	1H Detected 13C Echo Planar Imaging. Journal of Magnetic Resonance, 2002, 155, 64-71.	2.1	9
171	Cortical Responses to Single Mechanoreceptive Afferent Microstimulation Revealed with fMRI. NeuroImage, 2001, 13, 613-622.	4.2	47
172	Functional magnetic resonance imaging measurements of sound-level encoding in the absence of background scanner noise. Journal of the Acoustical Society of America, 2001, 109, 1559-1570.	1.1	81
173	Representation of Pleasant and Aversive Taste in the Human Brain. Journal of Neurophysiology, 2001, 85, 1315-1321.	1.8	605
174	A novel application of NMR microscopy: measurement of water diffusion inside bioadhesive bonds. Magnetic Resonance Imaging, 2001, 19, 487-488.	1.8	9
175	Single-shotT*2 measurement to establish optimum echo time for fMRI: Studies of the visual, motor, and auditory cortices at 3.0 T. Magnetic Resonance in Medicine, 2001, 45, 930-933.	3.0	33
176	Imaging the Long-Range Dipolar Field in Structured Liquid State Samples. Journal of Magnetic Resonance, 2001, 150, 147-155.	2.1	44
177	Dynamics of the nuclear magnetic resonance COSY-revamped by asymmetricz-gradients (CRAZED) experiment. Journal of Chemical Physics, 2001, 114, 10854-10859.	3.0	30
178	Sensory-specific satiety-related olfactory activation of the human orbitofrontal cortex. NeuroReport, 2000, 11, 893-897.	1.2	364
179	Sensory-specific satiety-related olfactory activation of the human orbitofrontal cortex. NeuroReport, 2000, 11, 399-403.	1.2	224
180	Time-course of the auditory BOLD response to scanner noise. Magnetic Resonance in Medicine, 2000, 43, 601-606.	3.0	94

#	Article	IF	CITATIONS
181	Modulation and task effects in auditory processing measured using fMRI. Human Brain Mapping, 2000, 10, 107-119.	3.6	116
182	Analytic calculations of the E-fields induced by time-varying magnetic fields generated by cylindrical gradient coils. Magnetic Resonance in Medicine, 2000, 44, 782-790.	3.0	43
183	Sound-Level Measurements and Calculations of Safe Noise Dosage During EPI at 3 T. Journal of Magnetic Resonance Imaging, 2000, 12, 157-163.	3.4	110
184	Open access birdcage coils for microscopic imaging of plants at 11.7 T. Magnetic Resonance Materials in Physics, Biology, and Medicine, 2000, 10, 69-74.	2.0	1
185	Dual resonant birdcage coils for1H detected13C microscopic imaging at 11.7 T. Magnetic Resonance Materials in Physics, Biology, and Medicine, 2000, 10, 61-68.	2.0	3
186	Open access birdcage coils for microscopic imaging of plants at 11.7T. Magnetic Resonance Materials in Physics, Biology, and Medicine, 2000, 10, 69-74.	2.0	3
187	Lip-Reading Ability and Patterns of Cortical Activation Studied Using fMRI. International Journal of Audiology, 2000, 34, 225-230.	0.7	39
188	Spatial and temporal distribution of solutes in the developing carrot taproot measured at single-cell resolution. Journal of Experimental Botany, 2000, 51, 567-577.	4.8	32
189	fMRI of the Responses to Vibratory Stimulation of Digit Tips. NeuroImage, 2000, 11, 188-202.	4.2	209
190	Dual resonant birdcage coils for 1H detected 13C microscopic imaging at 11.7 T. Magnetic Resonance Materials in Physics, Biology, and Medicine, 2000, 10, 61-68.	2.0	5
191	Time-course of the auditory BOLD response to scanner noise. Magnetic Resonance in Medicine, 2000, 43, 601.	3.0	2
192	Automatic compensation of motion artifacts in MRI. Magnetic Resonance in Medicine, 1999, 41, 163-170.	3.0	108
193	Analytic approach to the design of transverse gradient coils with co-axial return paths. Magnetic Resonance in Medicine, 1999, 41, 600-608.	3.0	36
194	The effect of scanner sound in visual, motor, and auditory functional MRI. Magnetic Resonance in Medicine, 1999, 41, 1230-1235.	3.0	78
195	Detecting activations in event-related fMRI using analysis of variance. Magnetic Resonance in Medicine, 1999, 42, 1117-1122.	3.0	54
196	sparse? temporal sampling in auditory fMRI. Human Brain Mapping, 1999, 7, 213-223.	3.6	801
197	Continuous saturation EPI with diffusion weighting at 3.0 T. NMR in Biomedicine, 1999, 12, 440-450.	2.8	11
198	Fetal brain activity demonstrated by functional magnetic resonance imaging. Lancet, The, 1999, 354, 645-646.	13.7	120

#	Article	IF	CITATIONS
199	The representation of pleasant touch in the brain and its relationship with taste and olfactory areas. NeuroReport, 1999, 10, 453-459.	1.2	411
200	"sparse―temporal sampling in auditory fMRI. , 1999, 7, 213.		2
201	Magnetic resonance imaging of controlled release pharmaceutical dosage forms. Pharmaceutical Science & Technology Today, 1998, 1, 32-39.	0.7	57
202	Multilayer Gradient Coil Design. Journal of Magnetic Resonance, 1998, 131, 286-294.	2.1	43
203	Investigation of Carbohydrate Metabolism and Transport in Castor Bean Seedlings by CyclicJCross Polarization Imaging and Spectroscopy. Journal of Magnetic Resonance, 1998, 132, 109-124.	2.1	39
204	In vivo perfusion measurements in the human placenta using echo planar imaging at 0.5 T. Magnetic Resonance in Medicine, 1998, 40, 467-473.	3.0	72
205	In Vivo Relaxation Time Measurements in the Human Placenta Using Echo Planar Imaging at 0.5 T. Magnetic Resonance Imaging, 1998, 16, 241-247.	1.8	51
206	Self-diffusion and molecular mobility in PVA-based dissolution-controlled systems for drug delivery. Magnetic Resonance Imaging, 1998, 16, 691-694.	1.8	22
207	Fluid transport in glass beads phantoms: spatial velocity measurements and confirmation of the stochastic model. Magnetic Resonance Imaging, 1998, 16, 605-607.	1.8	1
208	Strong gradients for spatially resolved diffusion measurements. Magnetic Resonance Imaging, 1998, 16, 587-591.	1.8	9
209	Echo-Planar Imaging Hardware. , 1998, , 31-64.		2
210	Measuring Patterson functions of inhomogeneous liquids using the nuclear dipolar field. Journal of Chemical Physics, 1997, 107, 702-706.	3.0	17
211	Nuclear magnetic resonance microscopy in liquids using the dipolar field. Journal of Chemical Physics, 1997, 106, 467-476.	3.0	40
212	Functional magnetic resonance imaging of single motor events reveals human presupplementary motor area. Annals of Neurology, 1997, 42, 632-637.	5.3	136
213	Structure and behavior in hydrophilic matrix sustained release dosage forms: 4. Studies of water mobility and diffusion coefficients in the gel layer of HPMC tablets using NMR imaging. Pharmaceutical Research, 1996, 13, 376-380.	3.5	108
214	Echo-planar microscopy of porous rocks. Magnetic Resonance Imaging, 1996, 14, 875-877.	1.8	13
215	Structural Investigations with the Dipolar Demagnetizing Field in Solution NMR. Physical Review Letters, 1996, 76, 4971-4974.	7.8	75
216	Active Acoustic Screening: Reduction of Noise in Gradient Coils by Lorentz Force Balancing. Magnetic Resonance in Medicine, 1995, 33, 276-281.	3.0	84

#	Article	IF	CITATIONS
217	NMR Microscopy of Single Neurons Using Spin Echo and Line Narrowed 2DFT Imaging. Magnetic Resonance in Medicine, 1995, 33, 790-794.	3.0	39
218	A robust single-shot partial sampling scheme. Magnetic Resonance in Medicine, 1995, 34, 74-79.	3.0	4
219	Quite transverse gradiant coils: Lorentz force balanced designs using geometrical similitude. Magnetic Resonance in Medicine, 1995, 34, 494-497.	3.0	46
220	Magic-Angle Gradient-Coil Design. Journal of Magnetic Resonance Series A, 1995, 115, 55-59.	1.6	16
221	A Modified Imaging Sequence for Accurate T2 Measurements Using NMR Microscopy. Journal of Magnetic Resonance Series B, 1995, 109, 66-69.	1.6	36
222	Active acoustic screening: design principles for quiet gradient coils in MRI. Measurement Science and Technology, 1994, 5, 1021-1025.	2.6	46
223	NMR microscopy of hydrating hydrophilic matrix pharmaceutical tablets. Magnetic Resonance Imaging, 1994, 12, 361-364.	1.8	61
224	Structure and behaviour in hydrophilic matrix sustained release dosage forms: 2. NMR-imaging studies of dimensional changes in the gel layer and core of HPMC tablets undergoing hydration. Journal of Controlled Release, 1994, 31, 121-128.	9.9	143
225	High-resolution echo-planar imaging at 3.0 T. Magnetic Resonance Materials in Physics, Biology, and Medicine, 1994, 2, 241-245.	2.0	16
226	Gastric motility by tagged EPI. Magnetic Resonance Materials in Physics, Biology, and Medicine, 1994, 2, 295-298.	2.0	12
227	Functional brain imaging using EPI at 3 T. Magnetic Resonance Materials in Physics, Biology, and Medicine, 1994, 2, 347-349.	2.0	5
228	Biplanar gradient coil design by simulated annealing. Magnetic Resonance Materials in Physics, Biology, and Medicine, 1994, 2, 387-389.	2.0	15
229	Active screening in RF coil design. Magnetic Resonance Materials in Physics, Biology, and Medicine, 1994, 2, 391-392.	2.0	1
230	NMR microscopy of single neurons at 500 MHZ. Magnetic Resonance Materials in Physics, Biology, and Medicine, 1994, 2, 445-447.	2.0	1
231	Measurement of GI water content using EPI at 0.5 tesla. Magnetic Resonance Materials in Physics, Biology, and Medicine, 1994, 2, 471-473.	2.0	5
232	Magnetic resonance imaging: Applications of novel methods in studies of porous media. Magnetic Resonance Imaging, 1992, 10, 741-746.	1.8	17
233	Ingress of water into solid nylon 6.6. Journal of Magnetic Resonance, 1992, 99, 507-524.	0.5	15
234	Indirect detection via the dipolar demagnetizing field. Journal of Magnetic Resonance, 1992, 100, 1-17.	0.5	28

#	Article	IF	CITATIONS
235	Ingress of water into solid nylon: Diffusion studies by NMR imaging. Magnetic Resonance Imaging, 1991, 9, 763-765.	1.8	6
236	Multiple spin echoes in multicomponent liquids. Journal of Magnetic Resonance, 1991, 93, 516-532.	0.5	14
237	Gradient coil design using active magnetic screening. Magnetic Resonance in Medicine, 1991, 17, 15-21.	3.0	57
238	Multiple spin echoes in liquids in a high magnetic field. Journal of Magnetic Resonance, 1990, 88, 643-651.	0.5	101
239	Screened coil designs for NMR imaging in magnets with transverse field geometry. Measurement Science and Technology, 1990, 1, 431-439.	2.6	24
240	Proton chemical-shift mapping using PREP. Journal of Magnetic Resonance, 1989, 82, 634-639.	0.5	3
241	CYCLCROP Mapping of13C Labelled Compounds: Perspectives in Polymer Science and Plant Physiology. , 0, , 21-52.		2